Synchronized asperities nucleate earthquakes on laboratory faults

Monica Barbery, Greg Hirth, and Terry Tullis

Department of Earth, Environmental, and Planetary Sciences, Brown University, Providence, RI, USA

ABSTRACT

Abundant heterogeneity has been documented on faults in nature across a wide range of length scales, including structural, mineralogical, and roughness variations. The role of complex heterogeneity on fault mechanics and frictional stability is not well established and experiments investigating heterogeneity have typically incorporated a single source of heterogeneity. Here, we conduct rock friction experiments on rough, bimaterial creeping faults to explore the role of lithological heterogeneity on fault mechanics and stability. When asperities juxtapose talc gouge, stable sliding occurs with a low friction coefficient, μ. Encounters of strong diabase asperities on rough, talc gouge-lined faults initiate dramatic increases in μ and transitions to unstable sliding characterized by frequent stick-slip events, StSEs. Seismic moments and stress drops of StSEs decrease as roughness increases. Intense mechanical damage limits the longevity of roughness rendering fault-asperities mechanically insignificant after multiple encounters. Encounters of strong, velocity weakening asperities provide a model to explain the nucleation of both seismic and aseismic slip events on nominally stable, creeping faults.

INTRODUCTION

Faults are structurally complex in nature with abundant heterogeneity from the microscopic scale up to the kilometer scale (Chester et al., 1993; Faulkner et al., 2003). Motion or slip along a fault is regulated by frictional processes with some faults exhibiting both seismic and aseismic slip (Miyazaki et al., 2011; Thomas et al., 2014; Avouac, 2015; Caballero et al., 2021). Fault slip can be simplified to three mechanical states: a locked state where no slip occurs, a stable sliding state dominated by slow slip, and an unstable sliding state dominated by fast slip. Identifying factors that govern the transition between these states is key to advancing our understanding of fast and slow earthquake mechanics and can inform other frictionally governed geologic processes including landslides and glacial flow. Two potentially important factors relate to sources of heterogeneity: roughness and mineralogy.

Fault roughness is well documented from the km- to µm-scale (Bistacchi et al., 2011; Candela et al., 2012). Roughness is thought to regulate the distribution of stress on faults (Candela et al., 2011; Fang and Dunham, 2013; Cattania and Segall, 2021). Kilometer scale roughness has been linked to megathrust and shallow subduction zone earthquakes (Bilek and Lay, 2002; Kirkpatrick et al., 2020), earthquake swarms (Cochran et al., 2023), and nucleation of secondary rupture fronts (Xu et al., 2024). Large-scale roughness has also been suggested as a mechanism to promote fault locking leading to earthquake nucleation (Lee et al., 2024). Though there is consensus that roughness is mechanically important, the role of roughness on frictional strength and stability is not clear. There are conflicting interpretations from laboratory experiments on whether roughness promotes frictional instabilities (Eijsink et al., 2022; Goebel et al., 2023) or inhibits them (Fryer et al., 2022; Xu et al., 2023). Other experimental investigations document transitional stability regimes but with conflicting interpretations on when roughness enhances or inhibits frictional instabilities (Harbord et al., 2017; Morad et al., 2022).

Experiments investigating mineralogical heterogeneities often combine frictionally strong, velocity weakening materials (μ decreases as velocity, V, increases) with frictionally weak, velocity strengthening materials (μ increases as V increases). These investigations show decreases in μ and increases in overall stability with increasing phyllosilicate content or when fabrics are present (Crawford et al., 2008; Collettini et al., 2009; Tembe et al., 2010; Moore and Lockner, 2011; Tesei et al., 2014; Hirauchi et al., 2023). More complex faults with distinct heterogeneous patches show decreased frictional stability on bimaterial faults compared to homogeneous faults (Bedford et al., 2022). In other experiments, long-term strengthening was documented and attributed to mixing of bimaterial patches (Arts et al., 2024).

As natural faults exhibit abundant heterogeneity, experiments that incorporate complex, multi-source heterogeneity can advance descriptions of fault mechanics and scaling of results from the lab to nature. We investigated the frictional properties of rough, bimaterial laboratory faults to explore the role of complex heterogeneity on frictional stability. The sliding surfaces of our experimental faults were engineered to facilitate direct links between slip-dependent mechanical behaviors and geometries of rough surfaces. To our knowledge, these are the first experiments to incorporate roughness and mineralogical heterogeneity simultaneously. We present mechanical and microstructural data from experiments and explore stability in the context of complex heterogeneity. Ultimately, we present a framework for transitions from stable to unstable sliding during fault creep that could nucleate seismic and aseismic slip events in nature including earthquakes, low frequency earthquakes, slow slip events, and tremor.

EXPERIMENTS

Experiments were performed using the Tullis Rotary Shear Apparatus[1] at Brown University at 25 MPa confining stress, 30 MPa normal stress, room temperature, and room humidity. We prepared annular samples of Frederick diabase with macroscopic asperities (Figure 1). The diabase is velocity weakening with a μ of 0.75 at the normal stress of our experiments. Between asperities, we packed a velocity strengthening talc gouge with a μ of 0.1. Coupling a talc gouge with the rough diabase has two benefits. Once at high normal stress, the gouge compacts relative to the initial sample geometry of Figure 1C, forcing asperities to ride over one another during encounters and allowing us to explore the role of roughness and mineralogy simultaneously. The contrasting mechanical behavior also allows us to distinguish the mechanical effects of each material.

To vary roughness, we used four geometries with amplitude to wavelength roughness ratios, R, of 0.007-0.003, representing the higher end of natural fault R that ranges from 0.01-0.0001 (Power and Tullis, 1991). We calculate R using asperity height divided by the circumferential length of an asperity and the clockwise gap before the next asperity and report the average for all lower sample asperities (Figure 1C). Experiments were conducted with symmetric roughness, R_S, or asymmetric roughness, R_A. In R_S experiments, the upper samples included seven symmetric asperities while the lower samples hosted seven, five or three asperities corresponding to average R_S of 0.007, 0.005 or 0.003. While the number of asperities decreased, the locations remained uniform ensuring all asperities enter and exit contact synchronously and lifetimes of asperity contacts are constant between all geometries (Figure 1B and 1C). This synchronicity and symmetry of asperities simplifies the identification of mechanical effects of roughness. For the R_A experiment, asperity locations were randomly permuted within 50° regions while maintaining an average R_A of 0.007. To isolate the mechanical effects of synchronizing asperities, and to limit velocity-dependent changes in wear rates (Boneh et al., 2013), a constant sliding velocity of 5 μm/s was maintained in all but one experiment. Experiments were conducted with total displacements, *d*, of 30 to 170 mm, allowing 1.5 to 7 asperity encounters, respectively.

RESULTS

When asperities interact on rough surfaces, rapid increases in μ trigger a shift from stable to unstable sliding with roughness controlling the peak μ and StSE characteristics (Figure 2). Stable sliding with a low μ dominated the first five mm of slip for all experiments when there was no diabase-diabase contact (Figure 2C). As the asperity mating index approached 1, representing fully mated asperities, μ increased, approaching diabase friction, and the fault transitioned from stable to unstable sliding characterized by frequent StSEs. The peak μ ranged from 0.78 to 0.6, decreasing with R_S. The increase in μ coincided with dilation at the sliding surface, with the magnitude of dilation increasing at higher R_S. As asperities unmated, μ decreased approaching the initial value and stable sliding resumed. This history repeated during a second asperity lifetime, though the μ peaks were reduced. Following the second lifetime, there was no significant change in μ with *d* or asperity mating index. Quasi-stable sliding was maintained for the remainder of slip with occasional instabilities at *d* up to 150 mm; μ always exceeded talc μ in all experiments. The amplitude of dilational events related to mating asperities decreased with *d* and decreasing R_S. By the seventh asperity lifetime, the amplitude of dilation during asperity encounters was significantly diminished.

StSEs occurred in all geometries, predominately during the first two asperity lifetimes (Figure 2A). When R_S was low, StSEs were most frequent as the asperity mating index increased and asperities entered contact. With larger R_S, StSEs were more frequent while the asperity mating index decreased (Figure 2D).

Representative microstructures from four experiments are shown in Figure 3. Pulverization and smoothing of the trailing and leading asperity edges was observed in all experiments. In low R_S experiments (Figures 3A and 3C), extensive, penetrating fracturing and pulverization occurred behind the asperity leading edges, with these regions elongating and connecting on one of the sample blocks. No widespread fracturing or pulverization was observed in high R_S experiments (Figures 3B and 3D). The overall degree of fracturing and pulverization did not vary significantly between low and high *d* experiments in either geometry.

DISCUSSION

When asperities interact on rough, bimaterial faults, the mechanical behavior of the fault reflects the mineralogy and abundance of asperities; outside of asperity encounters, the mechanical behavior is an intermediate between the two materials. In our experiments, talc comprises 71-80% of the sliding surface while diabase comprises 29-20% of the sliding surface. If μ is calculated using $\mu=\mu_{talc}P_{talc} + \mu_{diabase}P_{diabase}$ where P is the area percent, we would expect values of 0.29 to 0.23, averaging at 0.26. Instead, during the first asperity lifetime when diabase juxtaposed diabase (strong-strong contacts) μ increased dramatically approaching bare diabase values, though strong-strong contact area was only 29-12% of the sliding surface.

After the first asperity lifetime, μ decreased approaching the estimated aggregate estimates. Dramatic, though reduced, increases in μ occurred again during the second contact lifetime. The reduction in μ likely reflects a combination of mechanical damage that occurred during the first lifetime and smearing of talc along asperity surfaces. After this second lifetime, μ values remain low for the duration of sliding, reflecting intense mechanical damage during the first two lifetimes rendering asperities mechanically insignificant (Figure 3). In low R_S experiments, long-term μ is consistent with aggregate estimates. For the high R_S experiment, long-term μ was 0.5, exceeding the aggregate estimate of 0.29. This likely reflects mixing of pulverized diabase into the talc gouge due to the extensive damage at trailing and leading edges of asperities (Figure 3). Though more fracturing and pulverization occurs in lower R_S experiments, there are fewer asperities and upper sample asperities experience extended periods of no contact likely resulting in less mixing and a lower μ.

We calculated the seismic moment M_0 and cumulative moment for StSEs using $M_0 = GAd_e$ where G is the rigidity or shear modulus, A is the sliding surface area, and d_e is the StSE d. StSEs are defined as drops in μ of 0.005 or more during 0.5 μm of d. We used a G of 24 GPa, calculated from a proportional average of the values of G of 22 GPa for talc (Bailey and Holloway, 2000) and 30 GPa for diabase (Weijermars, 1997), an A of 729 mm^2 based on the sample dimensions assuming the entire interface slips when instabilities occur, and measured d for d_e. We also measured the shear stress drop, $\Delta\tau$, during StSEs.

Seismic moment and stress drop both increase with decreasing R_S, suggesting roughness increases stability (Figure 4). StSEs presumably reflect cataclastic failure at critically stressed microscopic asperity contacts located on strong-strong contacts. Inhomogeneous normal stress distributions have been documented in experiments on granite (Barbery et al., 2023). Since decreasing roughness lowers the total strong-strong contact area, if stresses are localized on strong-strong asperities, decreasing roughness increases the stress concentration at each strong-strong contact. These larger normal and shear stresses at microscopic asperities prior to failure would explain lager stress drops and seismic moments with lower roughness, since critical stiffness increases with normal stress. With reduced strong-strong contact area there may also be fewer asperities to serve as barriers to arrest or slow slip when asperities fail.

Concentrated stresses could also explain the different timing of StSEs. With larger R_S, increased strong-strong contact area may result in sufficiently distributed initial stresses preventing early StSEs. As illustrated in Fig 2D, microscopic asperities tend to fail as strong-strong contact area is reduced during unmating. In contrast, when R_S is low and strong-strong contact area is reduced, StSEs are more prevalent as asperities enter contact, suggesting stresses are sufficiently concentrated to induce failure. Mechanical damage due to early StSEs may alleviate stress concentrations during unmating and explain why instabilities do not recommence. The late StSEs in experiment 404 (Figure 4A) likely reflect a lack of mechanical damage; in this experiment asperities were initially mated with no mechanical damage prior to unmating and StSEs began as the mating index neared 0.

Cumulative moment was smaller for high R_S, and similar for intermediate to low R_S (Figure 4A) reflecting a balance between roughness magnitude and asperity longevity. When roughness is high, stress is sufficiently distributed to minimize damage and instabilities resulting in low cumulative moments and occasional StSEs after the first encounter. With intermediate to low roughness, stress is more localized resulting in numerous instabilities during the first 2-3 encounters, after which StSE frequency, M_0 and $\Delta\tau$ decrease. The maximum cumulative moment occurred in the asymmetric experiment and likely reflects a similar balance between magnitude and longevity of roughness enhanced by the complex asperity mating history during sliding.

This work demonstrates the complex mechanical behavior of heterogeneous faults. When frictionally stable, weak materials juxtapose strong or weak materials, stable sliding dominates. When frictionally strong asperities interact, the mechanical behavior alters dramatically, approaching the frictional behavior of the strong asperities. The average, peak μ decreased as R_S decreased. Assuming the peak μ is a function of the peak diabase μ of 0.79, and that changes in observed μ reflect changes in normal stress at asperities, this observation suggests normal stress increases by 120% and 140% as R_S decreases, in overall agreement with the decreased dilation and increased damage observed with decreasing R_S. Encounters of strong, velocity weakening asperities may promote the nucleation of seismic and aseismic events on nominally creeping faults. Whether failure occurs seismically or aseismically may depend on the size and rheology of asperities, with larger asperities nucleating earthquakes and smaller asperities nucleating slow slip or tremor. Similar processes may also contribute to landslide initiation. While synchronized strong-strong asperities can initiate rapid and dramatic transitions from stable to unstable sliding, asperities undergo extensive damage during encounters and become mechanically obsolete following multiple interactions.

ACKNOWLEDGEMENTS

This work was funded by the National Science Foundation (EAR-2052897).

REFERENCES CITED

Arts, J.P.B., Niemeijer, A.R., Drury, M.R., Willingshofer, E., and Matenco, L.C., 2024, The frictional strength and stability of spatially heterogeneous fault gouges: Earth and Planetary Science Letters, v. 628, p. 118586, doi:10.1016/j.epsl.2024.118586.

Avouac, J.-P., 2015, From Geodetic Imaging of Seismic and Aseismic Fault Slip to Dynamic Modeling of the Seismic Cycle: Annual Review of Earth and Planetary Sciences, v. 43, p. 233–271, doi:10.1146/annurev-earth-060614-105302.

Bailey, E., and Holloway, J.R., 2000, Experimental determination of elastic properties of talc to 800≥C, 0.5 GPa; calculations of the effect on hydrated peridotite, and implications for cold subduction zones: Earth and Planetary Science Letters, v. 183, p. 487–498.

Barbery, M.R., Chester, F.M., and Chester, J.S., 2023, Investigating Dynamic Weakening in Laboratory Faults Using Multi-Scale Flash Heating Coupled With mm-Scale Contact Evolution: Journal of Geophysical Research: Solid Earth, v. 128, p. e2023JB027110, doi:10.1029/2023JB027110.

Bedford, J.D., Faulkner, D.R., and Lapusta, N., 2022, Fault rock heterogeneity can produce fault weakness and reduce fault stability: Nature Communications, v. 13, p. 326, doi:10.1038/s41467-022-27998-2.

Bilek, S.L., and Lay, T., 2002, Tsunami earthquakes possibly widespread manifestations of frictional conditional stability: Geophysical Research Letters, v. 29, doi:10.1029/2002GL015215.

Bistacchi, A., Griffith, W.A., Smith, S.A.F., Di Toro, G., Jones, R., and Nielsen, S., 2011, Fault Roughness at Seismogenic Depths from LIDAR and Photogrammetric Analysis: Pure and Applied Geophysics, v. 168, p. 2345–2363, doi:10.1007/s00024-011-0301-7.

Boneh, Y., Sagy, A., and Reches, Z., 2013, Frictional strength and wear-rate of carbonate faults during high-velocity, steady-state sliding: Earth and Planetary Science Letters, v. 381, p. 127–137, doi:10.1016/j.epsl.2013.08.050.

Caballero, E., Chounet, A., Duputel, Z., Jara, J., Twardzik, C., and Jolivet, R., 2021, Seismic and Aseismic Fault Slip During the Initiation Phase of the 2017 MW = 6.9 Valparaíso Earthquake: Geophysical Research Letters, v. 48, p. e2020GL091916, doi:10.1029/2020GL091916.

Candela, T., Renard, F., Klinger, Y., Mair, K., Schmittbuhl, J., and Brodsky, E.E., 2012, Roughness of fault surfaces over nine decades of length scales: Journal of Geophysical Research: Solid Earth, v. 117, p. 2011JB009041, doi:10.1029/2011JB009041.

Candela, T., Renard, F., Schmittbuhl, J., Bouchon, M., and Brodsky, E.E., 2011, Fault slip distribution and fault roughness: Fault slip distribution and fault roughness: Geophysical Journal International, v. 187, p. 959–968, doi:10.1111/j.1365-246X.2011.05189.x.

Cattania, C., and Segall, P., 2021, Precursory Slow Slip and Foreshocks on Rough Faults: Journal of Geophysical Research: Solid Earth, v. 126, p. e2020JB020430, doi:10.1029/2020JB020430.

Chester, F.M., Evans, J.P., and Biegel, R.L., 1993, Internal structure and weakening mechanisms of the San Andreas Fault: Journal of Geophysical Research: Solid Earth, v. 98, p. 771–786, doi:10.1029/92JB01866.

Cochran, E.S., Page, M.T., Van Der Elst, N.J., Ross, Z.E., and Trugman, D.T., 2023, Fault Roughness at Seismogenic Depths and Links to Earthquake Behavior: The Seismic Record, v. 3, p. 37–47, doi:10.1785/0320220043.

Collettini, C., Niemeijer, A., Viti, C., and Marone, C., 2009, Fault zone fabric and fault weakness: Nature, v. 462, p. 907–910, doi:10.1038/nature08585.

Crawford, B.R., Faulkner, D.R., and Rutter, E.H., 2008, Strength, porosity, and permeability development during hydrostatic and shear loading of synthetic quartz-clay fault gouge: Journal of Geophysical Research: Solid Earth, v. 113, p. 2006JB004634, doi:10.1029/2006JB004634.

Eijsink, A.M., Kirkpatrick, J.D., Renard, F., and Ikari, M.J., 2022, Fault surface morphology as an indicator for earthquake nucleation potential: Geology, v. 50, p. 1356–1360, doi:10.1130/G50258.1.

Fang, Z., and Dunham, E.M., 2013, Additional shear resistance from fault roughness and stress levels on geometrically complex faults: Journal of Geophysical Research: Solid Earth, v. 118, p. 3642–3654, doi:10.1002/jgrb.50262.

Faulkner, D.R., Lewis, A.C., and Rutter, E.H., 2003, On the internal structure and mechanics of large strike-slip fault zones: field observations of the Carboneras fault in southeastern Spain: Tectonophysics, v. 367, p. 235–251, doi:10.1016/S0040-1951(03)00134-3.

Fryer, B., Giorgetti, C., Passelègue, F., Momeni, S., Lecampion, B., and Violay, M., 2022, The Influence of Roughness on Experimental Fault Mechanical Behavior and Associated Microseismicity: Journal of Geophysical Research: Solid Earth, v. 127, p. e2022JB025113, doi:10.1029/2022JB025113.

Goebel, T.H.W., Brodsky, E.E., and Dresen, G., 2023, Fault Roughness Promotes Earthquake-Like Aftershock Clustering in the Lab: Geophysical Research Letters, v. 50, p. e2022GL101241, doi:10.1029/2022GL101241.

Harbord, C.W.A., Nielsen, S.B., De Paola, N., and Holdsworth, R.E., 2017, Earthquake nucleation on rough faults: Geology, v. 45, p. 931–934, doi:10.1130/G39181.1.

Hirauchi, K., Hibi, R., Shirahige, R., and Takemura, T., 2023, Effects of phyllosilicate content on the slip behavior of fault gouge: Insights from room-temperature friction experiments on quartz–talc mixtures: Tectonophysics, v. 857, p. 229845, doi:10.1016/j.tecto.2023.229845.

Kirkpatrick, J.D., Edwards, J.H., Verdecchia, A., Kluesner, J.W., Harrington, R.M., and Silver, E.A., 2020, Subduction megathrust heterogeneity characterized from 3D seismic data: Nature Geoscience, v. 13, p. 369–374, doi:10.1038/s41561-020-0562-9.

Lee, J., Tsai, V.C., Hirth, G., Chatterjee, A., and Trugman, D.T., 2024, Fault-network geometry influences earthquake frictional behaviour: Nature, v. 631, p. 106–110, doi:10.1038/s41586-024-07518-6.

Miyazaki, S., McGuire, J.J., and Segall, P., 2011, Seismic and aseismic fault slip before and during the 2011 off the Pacific coast of Tohoku Earthquake: Earth, Planets and Space, v. 63, p. 637–642, doi:10.5047/eps.2011.07.001.

Moore, D.E., and Lockner, D.A., 2011, Frictional strengths of talc-serpentine and talc-quartz mixtures: Journal of Geophysical Research, v. 116, p. B01403, doi:10.1029/2010JB007881.

Morad, D., Sagy, A., Tal, Y., and Hatzor, Y.H., 2022, Fault roughness controls sliding instability: Earth and Planetary Science Letters, v. 579, p. 117365, doi:10.1016/j.epsl.2022.117365.

Power, W.L., and Tullis, T.E., 1991, Euclidean and fractal models for the description of rock surface roughness: Journal of Geophysical Research: Solid Earth, v. 96, p. 415–424, doi:10.1029/90JB02107.

Tembe, S., Lockner, D.A., and Wong, T., 2010, Effect of clay content and mineralogy on frictional sliding behavior of simulated gouges: Binary and ternary mixtures of quartz, illite, and montmorillonite: Journal of Geophysical Research: Solid Earth, v. 115, p. 2009JB006383, doi:10.1029/2009JB006383.

Tesei, T., Collettini, C., Barchi, M.R., Carpenter, B.M., and Di Stefano, G., 2014, Heterogeneous strength and fault zone complexity of carbonate-bearing thrusts with possible implications for seismicity: Earth and Planetary Science Letters, v. 408, p. 307–318, doi:10.1016/j.epsl.2014.10.021.

Thomas, M.Y., Avouac, J., Champenois, J., Lee, J., and Kuo, L., 2014, Spatiotemporal evolution of seismic and aseismic slip on the Longitudinal Valley Fault, Taiwan: Journal of Geophysical Research: Solid Earth, v. 119, p. 5114–5139, doi:10.1002/2013JB010603.

Weijermars, R., 1997, Principles of rock mechanics: Netherlands, Alboran Science Publishing.

Xu, S., Fukuyama, E., Yamashita, F., Kawakata, H., Mizoguchi, K., and Takizawa, S., 2023, Fault strength and rupture process controlled by fault surface topography: Nature Geoscience, v. 16, p. 94–100, doi:10.1038/s41561-022-01093-z.

Xu, L., Ji, C., Meng, L., Ampuero, J.-P., Yunjun, Z., Mohanna, S., and Aoki, Y., 2024, Dual-initiation ruptures in the 2024 Noto earthquake encircling a fault asperity at a swarm edge: Science, v. 385, p. 871–876, doi:10.1126/science.adp0493.

FIGURES AND CAPTIONS

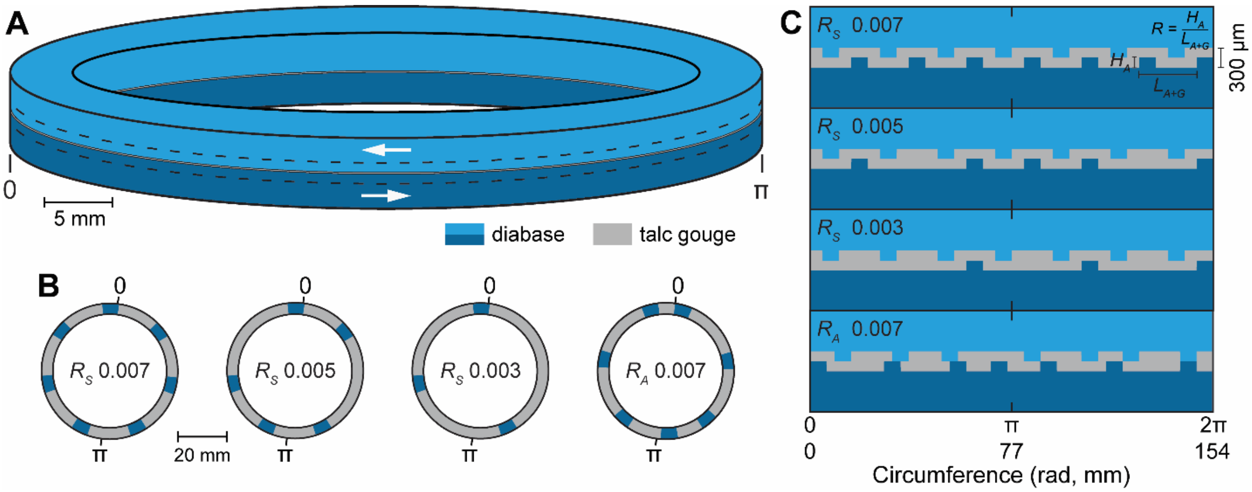

Figure 1. Initial sample geometries. A) Schematic view of annular samples showing the sense of slip. B) Lower sample sliding surfaces showing locations of diabase asperities (blue) and talc gouge (gray) for samples with symmetric or asymmetric roughness, R_S or R_A, respectively. Roughness is calculated using the average amplitude to wavelength ratio of asperities on the lower sample. C) Vertically exaggerated (25X) wraparound sections (dashed region in 1A) showing the initial asperity locations in each geometry. H_A = 150 μm.

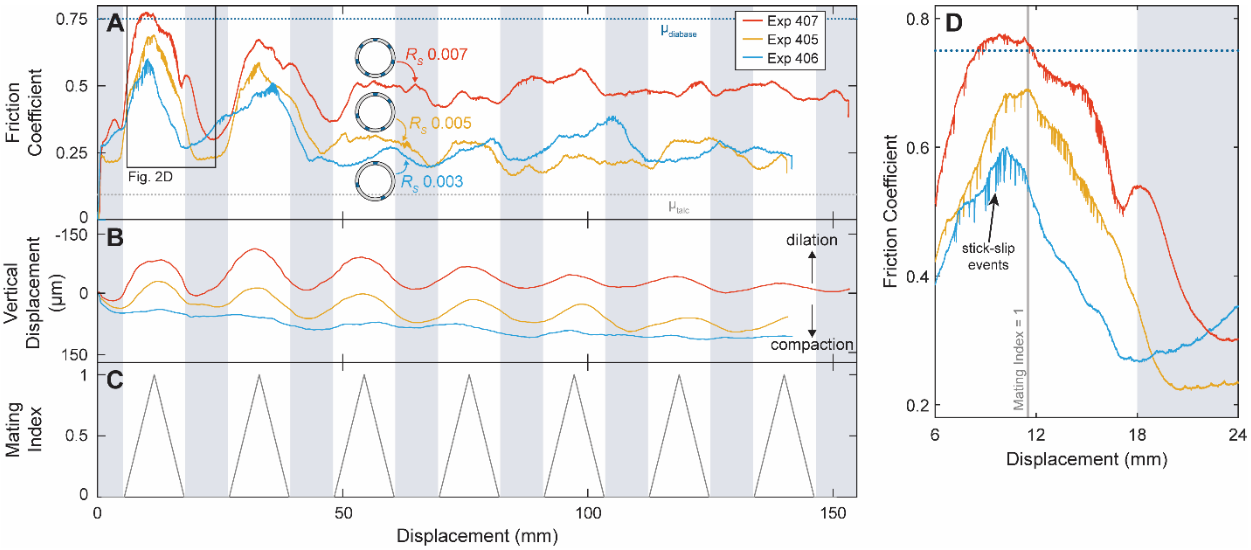

Figure 2. Representative mechanical results from three symmetric roughness experiments: 407 with a R_S of 0.007 (red), 405 with R_S of 0.005 (yellow), and 406 with R_S of 0.003 (blue). A) Measured coefficient of friction. B) Measured fault-normal displacement. C) Asperity mating index where 1 corresponds to fully mated asperities. D) Close up of μ during and following the first asperity encounter.

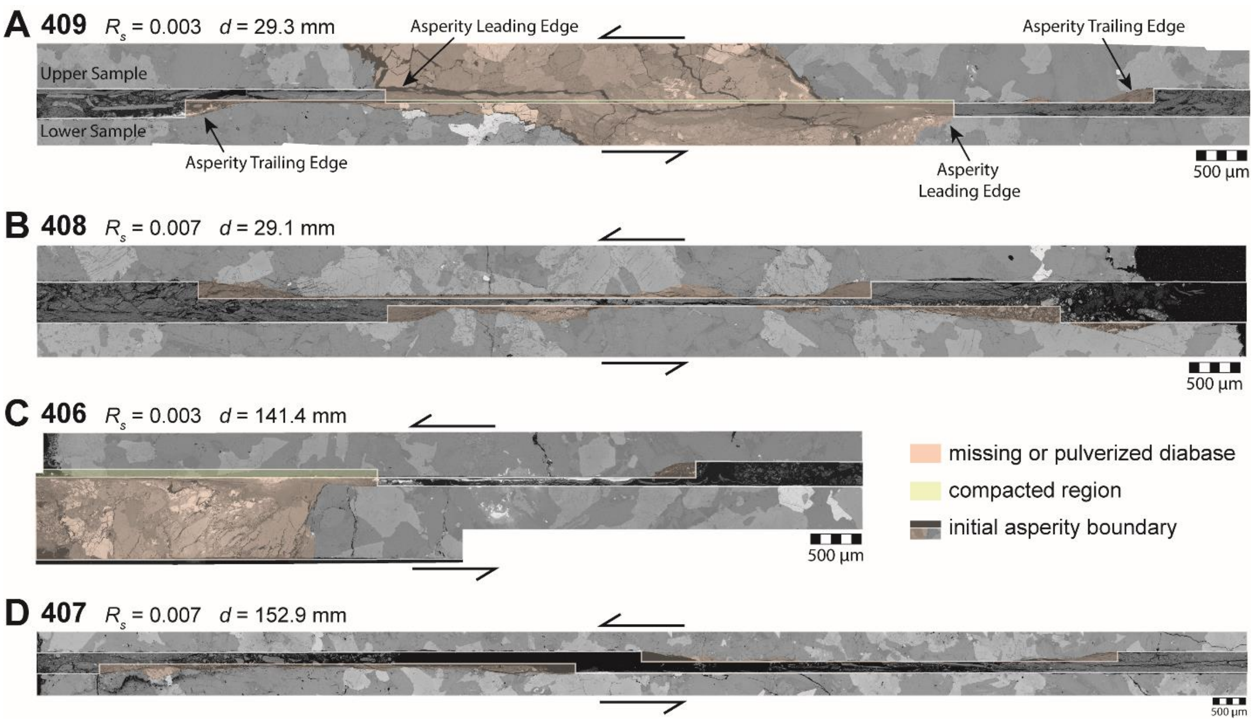

Figure 3. Scanning electron microscope images from four experiments. White lines map the original asperity boundaries. Arrows denote sense of slip for the upper and lower sample blocks. A and B) Asperities from experiment 409 (A) and 408 (B) after ~1.5 asperity encounters. C and D) Asperities from experiment 406 (C) and 407 (D) after ~6.5 and ~7 encounters, respectively.

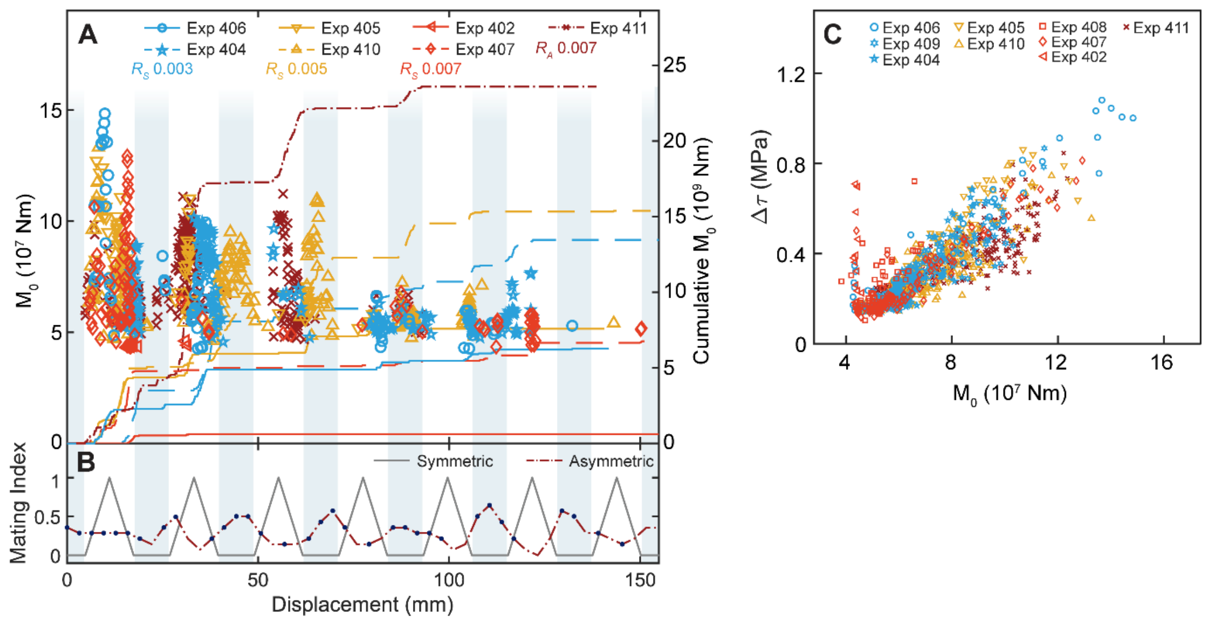

Figure 4. A) Seismic moments M_0 and cumulative M_0 calculated from StSEs. Two experiments from each symmetric geometry R_S are plotted alongside one asymmetric geometry R_A experiment. B) Asperity mating index values. Navy circles mark periods with one or more mated asperity in the asymmetric geometry. C) Measured shear stress drop $\Delta\tau$ versus M_0 for StSEs in 9 experiments.

[1]**Supplemental Material.** Additional data, results, apparatus details, and sample details are available. Please visit https://doi.org/10.1130/ to access the supplemental material; contact editing@geosociety.org with any questions.